

Accruement of nonlinear dynamical system and its dynamics: electronics and cryptographic engineering

*Najeeb Alam Khan^a, Muhammad Ali Qureshi^b,
Saeed Akber^a, and Tooba Hameed^a*

^aDepartment of Mathematics, University of Karachi, Karachi, Pakistan ^bDepartment of Physics,
University of Karachi, Karachi, Pakistan

8.1 Introduction

Chaos, a deterministic oscillation used to be treated as a random and stochastic phenomenon, incorporated a variety of ongoing natural phenomena in this world. Phenomena that have been shown to be stochastic include the physics of probing nuclear structure [1], the fusion plasma study [2], semiconductor lasers [3], the biological aspects of aging [4], medicine [5], population [6], forecasting in economics and finance [7,8], communication applications such as chaos with underwater communication [9], communication with laser [10], secure communication [11], antijamming [12], filtering of noise during communication [13], etc. The chaotic systems are identified and studied on the basis of time domain, space domain, and the number of space dimensions. The time domain of a system represents the properties of continuity and discreteness, whereas the space domain shows the real and complex nature of a system. The number of space dimensions in a chaotic system represents the number of differential equations used to engender a chaotic behavior. Usually, chaotic systems with continuous time domain and real space domain are described by a system of two differential equations like Van der Pole [14] and Duffing [15] or by three differential equations like Lorenz [16], Chua [17], Newton–Leipnik [18], etc. Hyperchaos generation in a real continuous system includes Lorenz [19], Chen [20], Rossler [21], etc.

In the last few years the fractional-order derivatives are focused persistently and are now an ongoing conundrum, especially considering the Laplace transform techniques with proper initial condition terms. This old calculus began with the question asked by L'Hôpital in 1695

(see [22,23]), which is related to the meaning of $\frac{d^n f}{dt^n}$ for $n = 0.5$. Before this, the concept and physical sense of mathematical representation was clear for integer values; however, the things started to get complicated by the stimulation of this aberrant question. Because of greater complexity of the nature, we may think of these noninteger derivatives as an acceptable norm. The fractional-order derivatives have got significant advantage over integer models and have robust and promising results on their “memory” [24–26] and heredity assets for different systems. The definition of fractional derivatives is still and unsolved riddle; scientists found their own methodologies and notation to express and fit the notion of noninteger derivatives. Among them, the most famous and popular definitions are proposed by Riemann and Liouville and by Grunwald and Letnikov; others include Liouville, Riezs, Riemann, Caputo, Weyl, Marchaud, Coimbra, Hadamard, and other definitions. Nowadays the fractional derivatives are applied in real-life applications such as the fractional-order PID controllers for industries [27], the compression deformation study in solid-state physics for polymers [28], the study of animal brain using MRI technique applied via fractional-order derivative and entropy [29], filtering processes of layers in magnetic fields with fractional-derivative separation filter [30], the encryption of voice, image, and gif in chaotic systems [31,32].

The revolution in information processing and secure telecommunication began with the 20th century and is now used firmly in the 21st century. The transfer of huge amount of data takes place between the people in the form of emails, messages, documents, voice notes; video calls, etc., and this requires privacy. Today cryptography is a fascinating field, which allows us to transfer our data more securely (end-to-end) without any hinderance. The data generated from the presented theoretical model along with fractional values are useful in the generation of random numbers, which allows us to secure a wider range of information for healthy communication.

In this work, we present a blend of two nonlinear oscillatory systems with fractional-order derivative. We study the mathematical model via its dynamical parameter in later section, with 2D graphs of time series of individual state variables, phase portraits, Poincaré maps, and bifurcation diagrams. We examine the system vividness via electronic realization using passive components (resistors, capacitors, multipliers, and operational amplifier) using Multisim. The nonlinear data are implemented on Python programming codes and also used to scramble the voice, image, and pdf text to ensure the cryptographic use of the engendered model.

8.2 Systems and their properties

Sambas et al. [33] presented the following three-dimensional chaotic system, which we call system A:

$$\begin{aligned} D^\gamma \phi_1(\tau) &= \phi_2(\tau) - \phi_1(\tau)\phi_3(\tau) - \phi_2(\tau)\phi_3(\tau), \\ D^\gamma \phi_2(\tau) &= a\phi_1(\tau)\phi_3(\tau), \\ D^\gamma \phi_3(\tau) &= \phi_2^2(\tau) - b\phi_3(\tau), \end{aligned} \tag{8.1}$$

where $\phi_1(\tau)$, $\phi_2(\tau)$, and $\phi_3(\tau)$ are state variables, a and b are control parameters with values $a = 2.8$ and $b = 0.6$, and the initial state values are $\phi_1(0) = 0.1$, $\phi_2(0) = 0.1$, and $\phi_3(0) = 0.1$.

For aggregation, we consider another chaotic system B presented by Chen and Lee [34] and defined as

$$\begin{aligned} D^\gamma \phi_1(\tau) &= -\phi_2(\tau)\phi_3(\tau) + c\phi_1(\tau), \\ D^\gamma \phi_2(\tau) &= \phi_1(\tau)\phi_3(\tau) + d\phi_2(\tau), \\ D^\gamma \phi_3(\tau) &= (1/3)\phi_1(\tau)\phi_2(\tau) + e\phi_3(\tau), \end{aligned} \quad (8.2)$$

where $\phi_1(\tau)$, $\phi_2(\tau)$, and $\phi_3(\tau)$ are state variables, c , d , and e are control parameters with the values $c = 3$, $d = -10$, and $e = -3.8$, and the initial state values are $\phi_1(0) = 0.2$, $\phi_2(0) = 0.2$, and $\phi_3(0) = 0.2$.

The aggregation of Eqs. (8.1) and (8.2) leads to the new generalized 3-D system with five-term quadratic nonlinearity of the form

$$\begin{aligned} D^\gamma \phi_1(\tau) &= \frac{1}{2}(\phi_2(\tau) - \phi_1(\tau)\phi_3(\tau) - 2\phi_2(\tau)\phi_3(\tau) + c\phi_1(\tau)), \\ D^\gamma \phi_2(\tau) &= \frac{1}{2}((a+1)\phi_1(\tau)\phi_3(\tau) + d\phi_2(\tau)), \\ D^\gamma \phi_3(\tau) &= \frac{1}{2}(\phi_2^2(\tau) - (b-e)\phi_3(\tau) + (1/3)\phi_1(\tau)\phi_2(\tau)), \end{aligned} \quad (8.3)$$

where $\phi_1(\tau)$, $\phi_2(\tau)$, and $\phi_3(\tau)$ are state variables, a , b , c , d , and e are control parameters with values $a = 2.8$, $b = 0.6$, $c = 3$, $d = -10$, and $e = -3.8$, and the initial state values are $\phi_1(0) = 0.15$, $\phi_2(0) = 0.15$, and $\phi_3(0) = 0.2$.

Here we implement the property of proportional fractional derivative of the differential operator $D^\gamma \phi(\tau)$ of order γ defined as

$$D^\gamma \phi(\tau) = \eta_1(\gamma, t)\phi(t) + \eta_0(\gamma, t). \quad (8.4)$$

Expression (8.4) transforms a fractional-order derivative into the form where the presence of integer-order derivative accurately reduces various complex computations.

Substitution of property (8.4) transforms the aggregated system (8.3) into equivalent integer form

$$\begin{aligned} \dot{\phi}_1(\tau) &= \frac{1}{\gamma} \left(\frac{1}{2}(\phi_2(\tau) - \phi_1(\tau)\phi_3(\tau) - 2\phi_2(\tau)\phi_3(\tau) + c\phi_1(\tau)) - (1-\gamma)\phi_1(\tau) \right), \\ \dot{\phi}_2(\tau) &= \frac{1}{\gamma} \left(\frac{1}{2}((a+1)\phi_1(\tau)\phi_3(\tau) + d\phi_2(\tau)) - (1-\gamma)\phi_2(\tau) \right), \\ \dot{\phi}_3(\tau) &= \frac{1}{\gamma} \left(\frac{1}{2}(\phi_2^2(\tau) - (b-e)\phi_3(\tau) + (1/3)\phi_1(\tau)\phi_2(\tau)) - (1-\gamma)\phi_3(\tau) \right), \end{aligned} \quad (8.5)$$

where $\phi_1(\tau)$, $\phi_2(\tau)$, and $\phi_3(\tau)$ are state variables, a , b , c , d , and e are control parameters with values $a = 2.8$, $b = 0.6$, $c = 3$, $d = -10$, and $e = -3.8$, and the initial state values are $\phi_1(0) = 0.15$, $\phi_2(0) = 0.15$, and $\phi_3(0) = 0.2$.

TABLE 8.1 Fixed (equilibrium) points and eigenvalues of system (8.5).

γ	Fixed points	Eigenvalues
1.00	$E_1(0, 0, 0)$	($-5, 2.2, 1.5$)
	$E_{2,3}(\mp 4.47254\iota, \pm 4.09273\iota, -2.43613)$	($-8.50 + 1.11 \times 10^{-15}\iota, 2.01 - 2.38\iota, 2.01 + 2.38\iota$)
	$E_{4,5}(\pm 3.49291, \pm 2.15069, 1.62034)$	($-8.21, 0.85 + 2.44\iota, 0.85 - 2.44\iota$)
0.98	$E_1(0, 0, 0)$	($-5.12, -2.27, 1.51$)
	$E_{2,3}(\mp 4.47254\iota, \pm 4.11373\iota, -2.43014)$	($-8.74 - 2.22 \times 10^{-16}\iota, 2.05 + 2.42\iota, 2.05 - 2.42\iota$)
	$E_{4,5}(\pm 3.52826, \pm 2.14877, 1.60909)$	($-8.42, 0.87 + 2.49\iota, 0.87 - 2.49\iota$)

TABLE 8.2 Lyapunov spectrums and Kaplan–Yorke dimension of aggregating system (8.5).

γ	Systems	Lyapunov spectrums	Kaplan–Yorke dimension
1.00	A system	(0.326819, 0.118090, -1.602272)	2.27767
	B system	(1.216154, -0.003434, -11.833265)	2.10248
	Aggregated system	(0.118651, -0.033128, -7.351012)	2.01163
0.98	A system	(0.334310, 0.089782, -1.632494)	2.25978
	B system	(0.957593, 0.2101137, -12.068991)	2.09675
	Aggregated system	(0.441744, -0.463327, -7.502352)	1.99712

The fixed points and eigenvalues of system (8.5) at different values of γ are calculated and arranged in Table 8.1. The graphical comparison of system A, B and aggregated system for different value of γ is presented by two-dimensional phase portraits. Firstly, for $\gamma = 1.00$, Figs. 8.1(a)–8.1(c) represent the phase diagrams of $(\phi_1(\tau), \phi_2(\tau))$, Figs. 8.2(a)–8.2(c) represent the phase diagrams of $(\phi_2(\tau), \phi_3(\tau))$, and Figs. 8.3(a)–8.3(c) represent the coordinates $(\phi_1(\tau), \phi_3(\tau))$. After this, our fractional-order system with decimal value 0.98 is executed using Eq. (8.5). Figs. 8.4(a)–8.4(c) represent the plot of $(\phi_1(\tau), \phi_2(\tau))$, Figs. 8.5(a)–8.5(c) represent the plot of $(\phi_2(\tau), \phi_3(\tau))$, and Figs. 8.6(a)–8.6(c) represent $(\phi_1(\tau), \phi_3(\tau))$. In Figs. 8.7(a)–8.7(c), we plot the Poincaré map of system (8.5) to represent the periodic nature of the system, as it returns back to the same region again and again.

8.2.1 Lyapunov spectrum and Kaplan–Yorke dimension

One of the chaotic system qualities is the Lyapunov spectrum, which describes the separation rate of infinitesimally closed trajectories. We calculated the Lyapunov spectrum of the presented chaotic system for both integer and fractional values of γ using Wolf's algorithm [35]. The system randomness can be perceived by the calculated values of Lyapunov exponents, i.e., for $\gamma = 1$, we have two negative values and one positive, and for $\gamma = 0.98$, the results remain consistent with chaos standards presented in Table 8.2.

8.3 Analog circuit imitations

In this section, we present the electronic realization of a nonlinear chaotic system. The design of circuital elements is theoretically accomplished through Multisim with passive

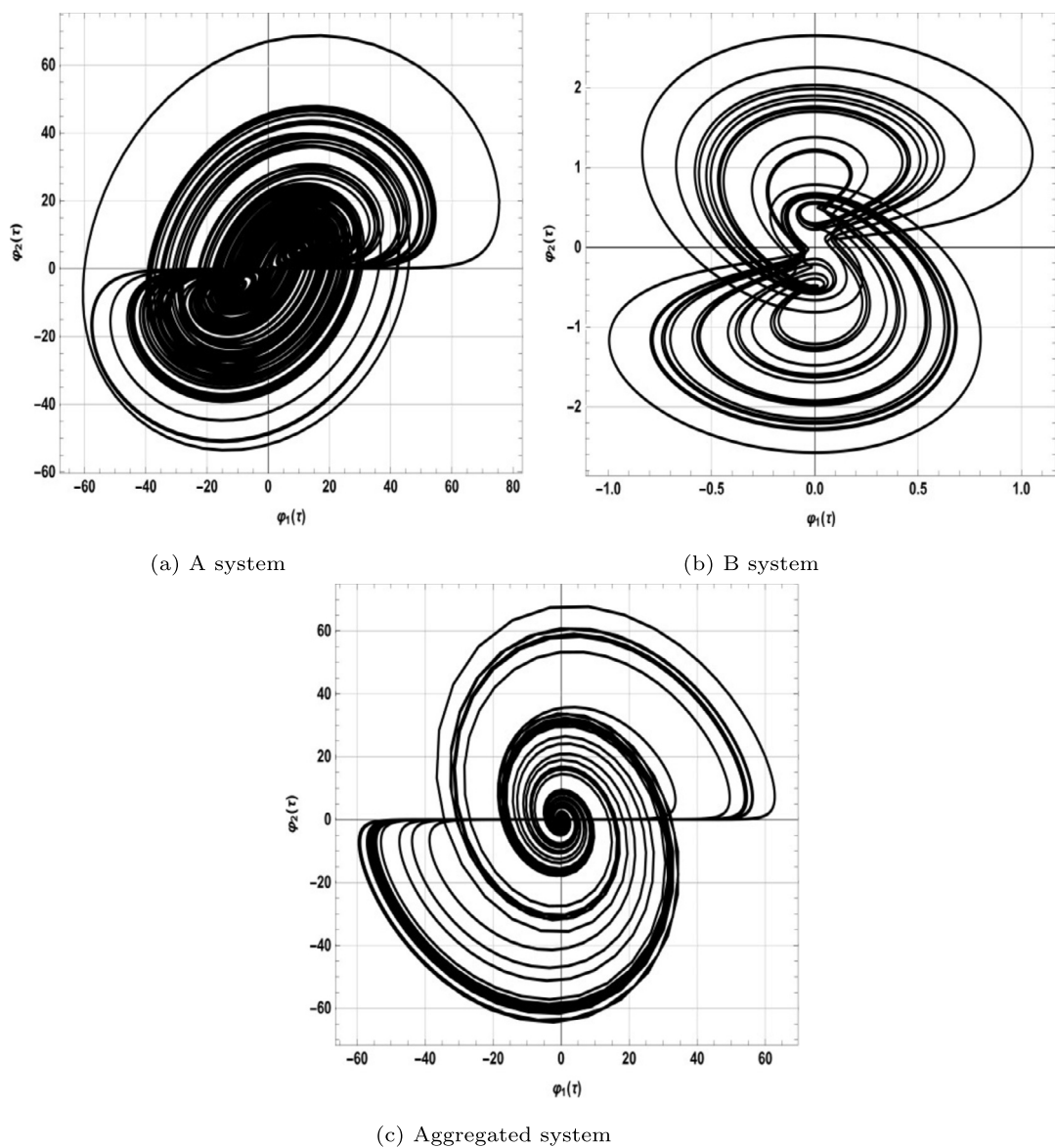


FIGURE 8.1 Phase portraits of (ϕ_1, ϕ_2) at $\gamma = 1$.

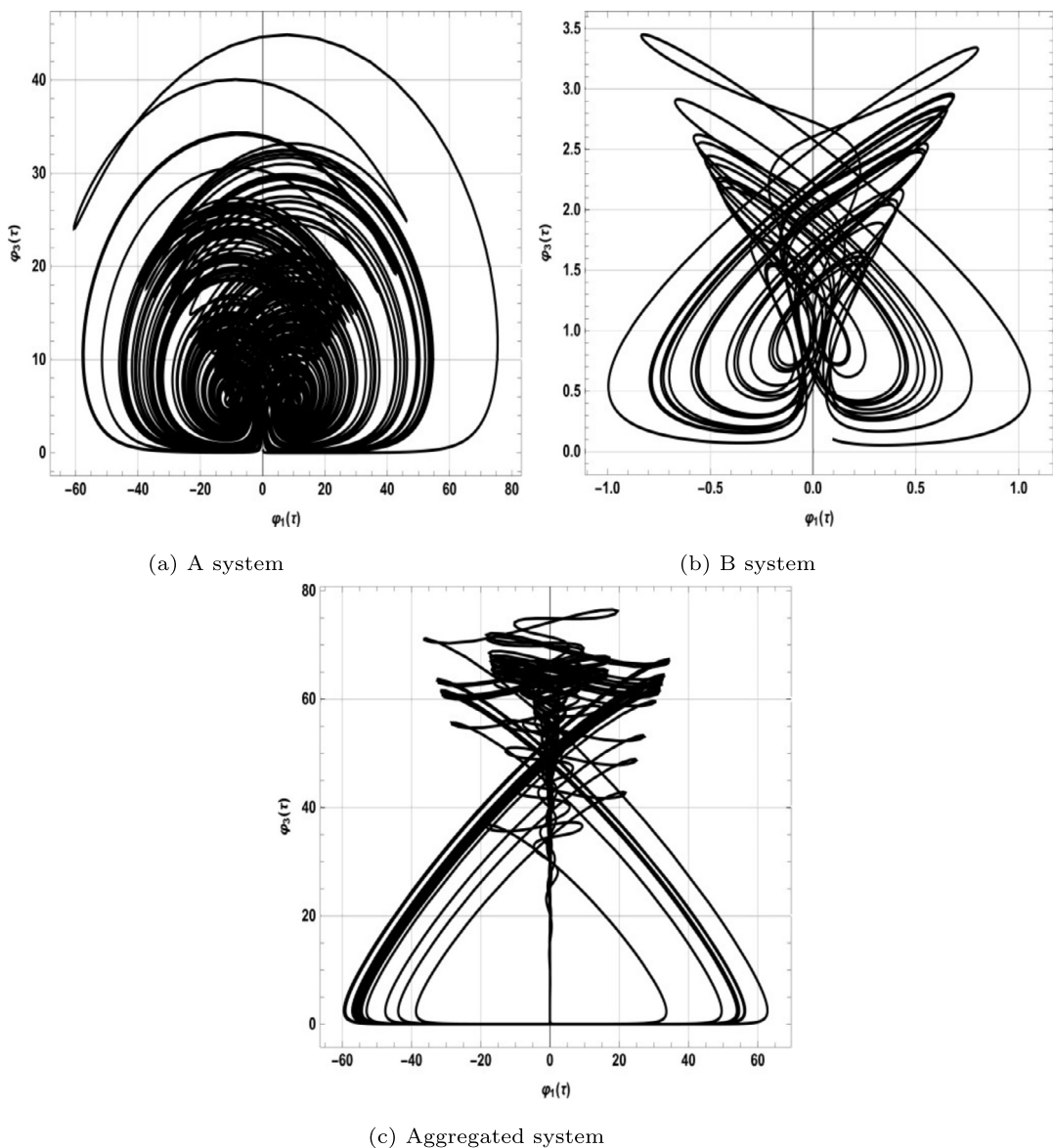


FIGURE 8.2 Phase portraits of (ϕ_1, ϕ_3) at $\gamma = 1$.

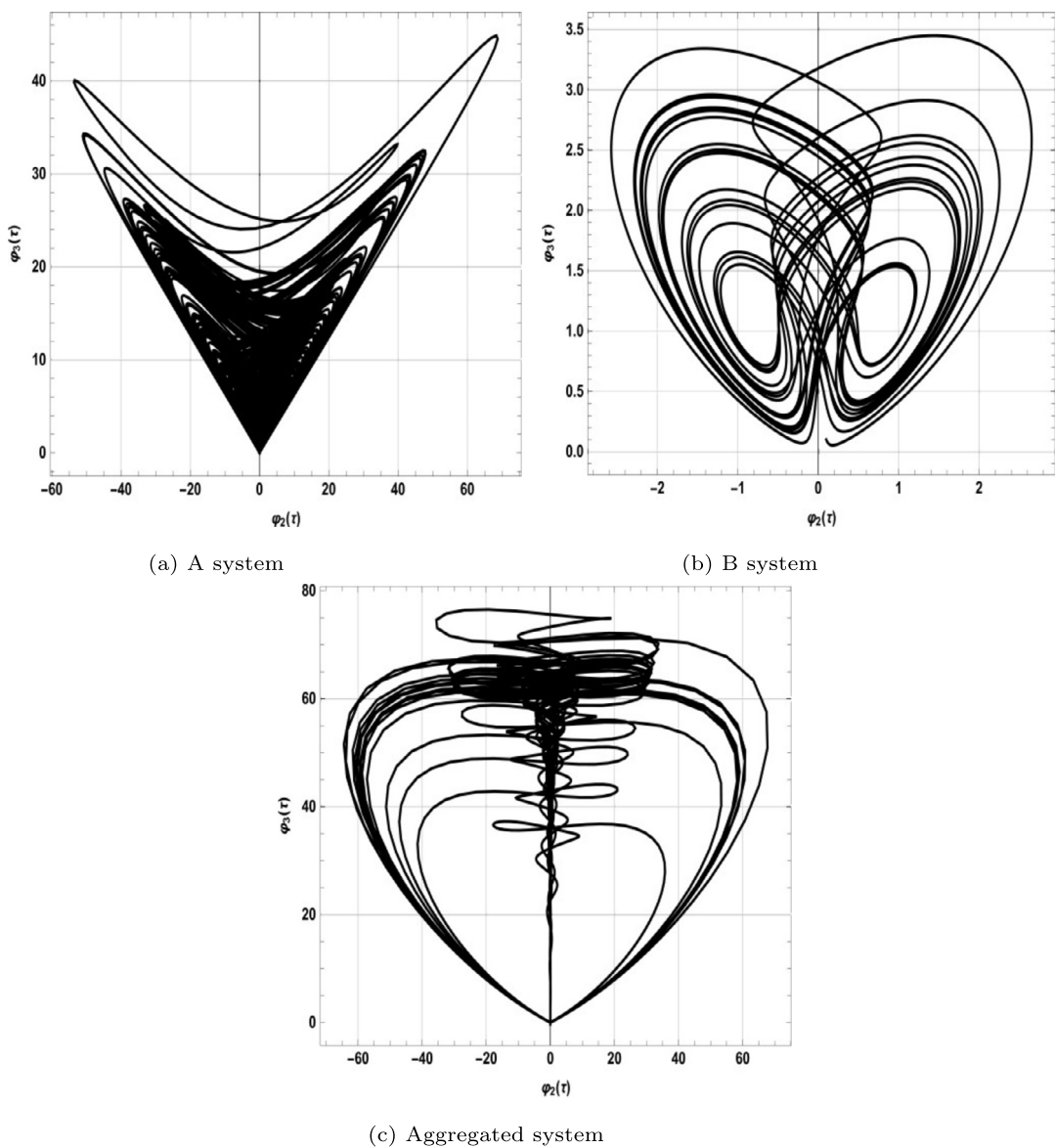


FIGURE 8.3 Phase portraits of (ϕ_2, ϕ_3) at $\gamma = 1$.

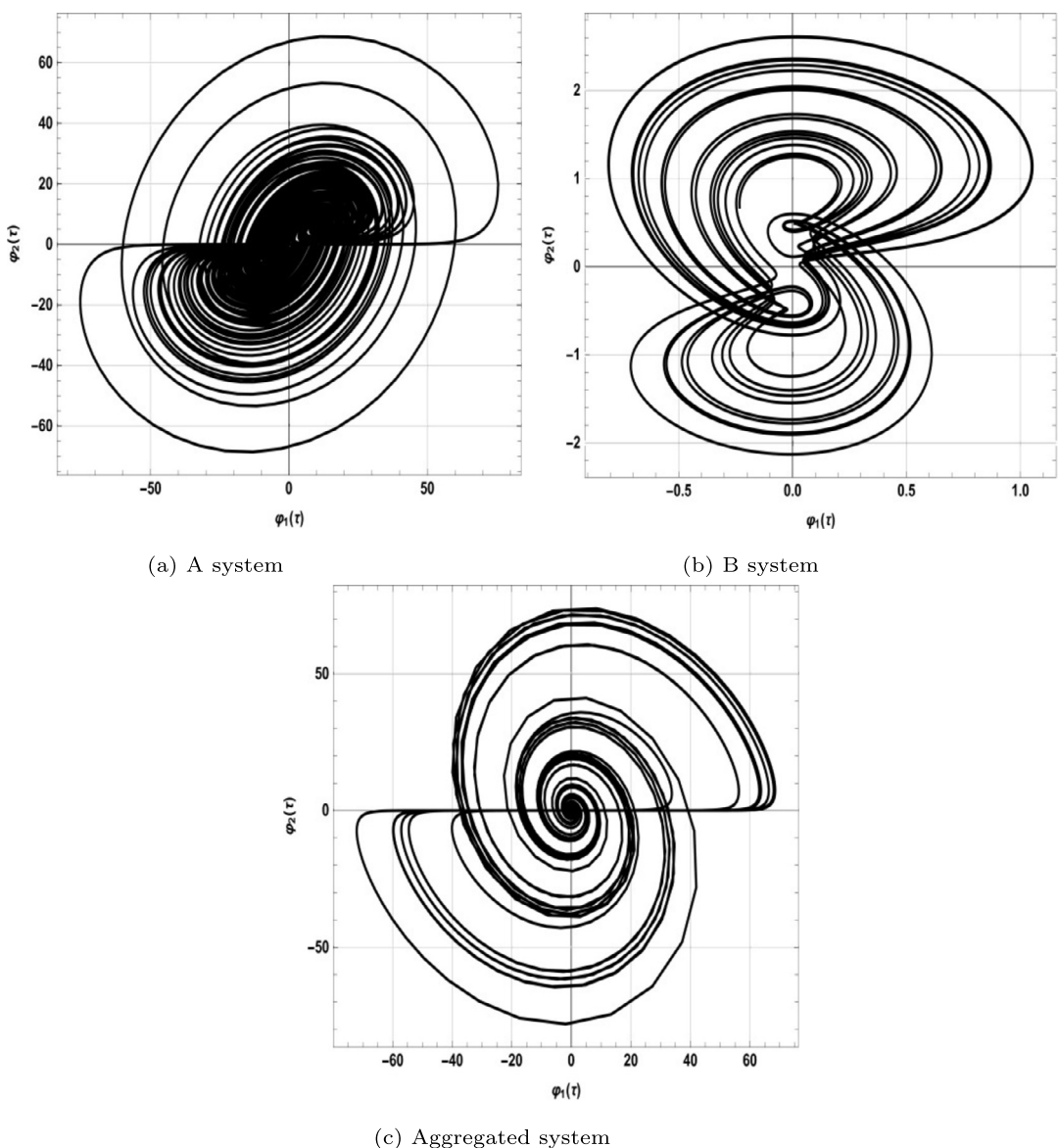


FIGURE 8.4 Phase portraits of (ϕ_1, ϕ_2) at $\gamma = 0.98$.

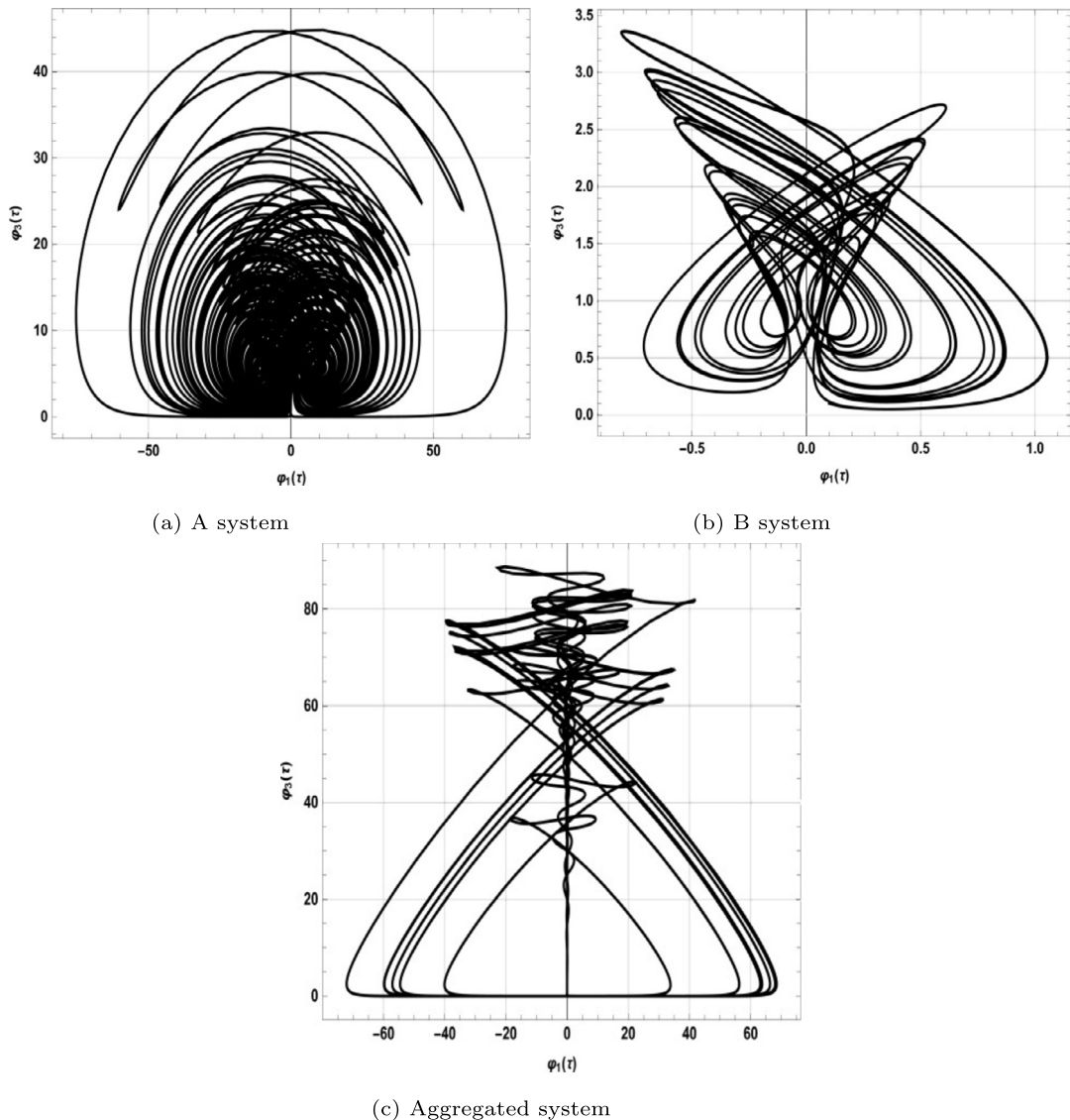


FIGURE 8.5 Phase portraits of (ϕ_1, ϕ_3) at $\gamma = 0.98$.

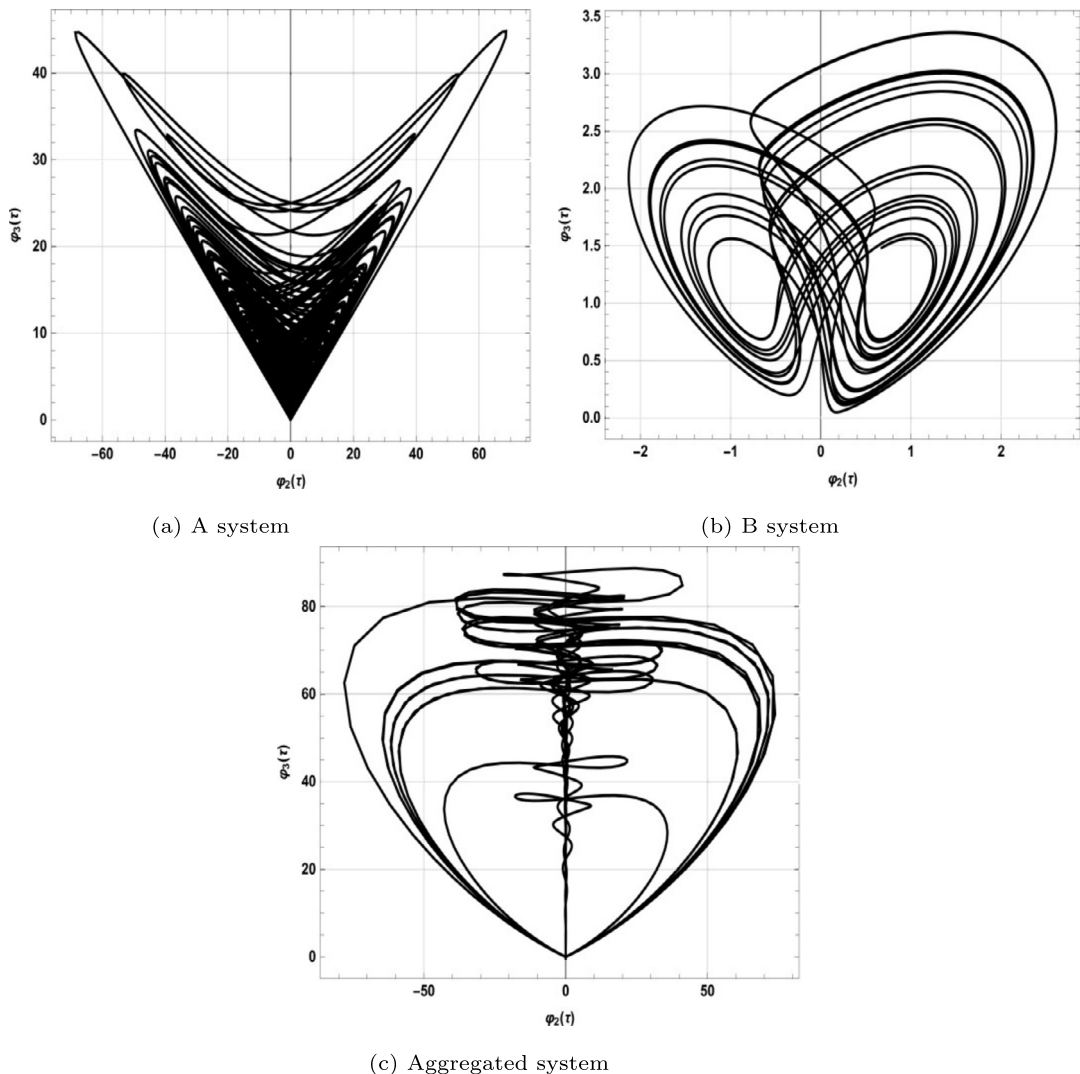
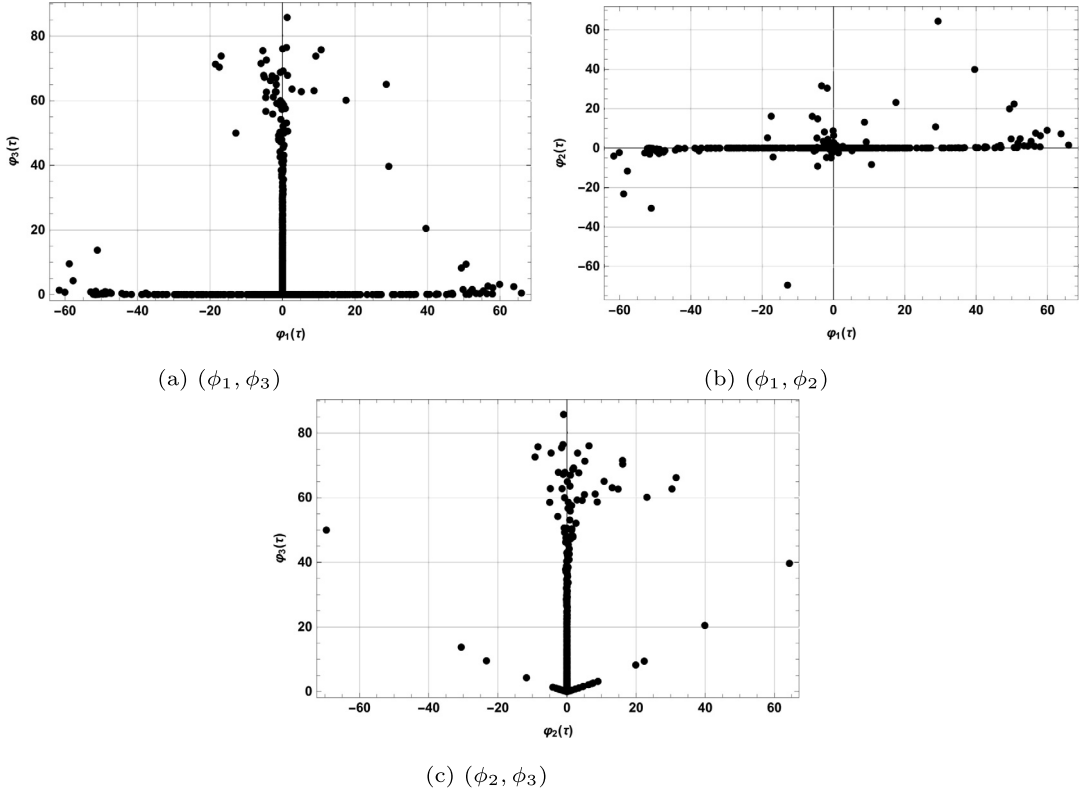


FIGURE 8.6 Phase portraits of (ϕ_2, ϕ_3) at $\gamma = 0.98$.

FIGURE 8.7 Poincaré plots of system (8.5) at $\gamma = 0.98$.

components like resistors, capacitors, multipliers, and operational amplifiers. The analog circuit represents the application of our chaotic system in the field of physics and electronic engineering. The circuital equation constructed using the Kirchhoff law for system (8.5) is

$$\begin{aligned}\dot{\phi}_1(\tau) &= \frac{1}{\gamma} \left(\frac{1}{2} \left(\frac{\phi_2(\tau)}{R_1 C_1} - \frac{\phi_1(\tau)\phi_3(\tau)}{R_2 C_1} - \frac{2\phi_2(\tau)\phi_3(\tau)}{R_3 C_1} + \frac{c\phi_1(\tau)}{R_4 C_1} \right) - \frac{(1-\gamma)\phi_1(\tau)}{R_5 C_1} \right), \\ \dot{\phi}_2(\tau) &= \frac{1}{\gamma} \left(\frac{1}{2} \left(\frac{(a+1)\phi_1(\tau)\phi_3(\tau)}{R_6 C_2} + \frac{d\phi_2(\tau)}{R_7 C_2} \right) - \frac{(1-\gamma)\phi_2(\tau)}{R_8 C_2} \right), \\ \dot{\phi}_3(\tau) &= \frac{1}{\gamma} \left(\frac{1}{2} \left(\frac{\phi_2^2(\tau)}{R_9 C_3} - \frac{(b-e)\phi_3(\tau)}{R_{10} C_3} + \frac{(1/3)\phi_1(\tau)\phi_2(\tau)}{R_{11} C_3} \right) - \frac{(1-\gamma)\phi_3(\tau)}{R_{12} C_3} \right),\end{aligned}\quad (8.6)$$

where ϕ_1 , ϕ_2 , ϕ_3 are the voltages across the capacitors C_1 , C_2 , and C_3 , respectively. The calculated values of resistors and capacitors are tabulated in Table 8.3, and the schematic electronics circuit of system (8.5) is given in Fig. 8.8. The output of oscilloscope is shown in Figs. 8.9(a)–8.9(c) with two-dimensional phase plots.

TABLE 8.3 Values of resistances used electronic circuit for different values of γ with capacitors C_1 , C_2 , and C_3 40 nF.

γ	Resistance (ohms)		γ	Resistance (ohms)	
1.00	R_1	50000.0	0.98	R_1	48499.99999999999
	R_2	5000.0		R_2	4850.0
	R_3	2500.0		R_3	2425.0
	R_4	8333.33333333333		R_4	8083.33333333332
	R_5	-		R_5	80833.3333333326
	R_6	657.8947368421053		R_6	638.1578947368422
	R_7	2500.0		R_7	2425.0
	R_8	-		R_8	80833.3333333326
	R_9	5000.0		R_9	4850.0
	R_{10}	5681.8181818182		R_{10}	5511.363636363636
	R_{11}	7499.99999999999		R_{11}	7274.999999999999
	R_{12}	-		R_{12}	80833.3333333326

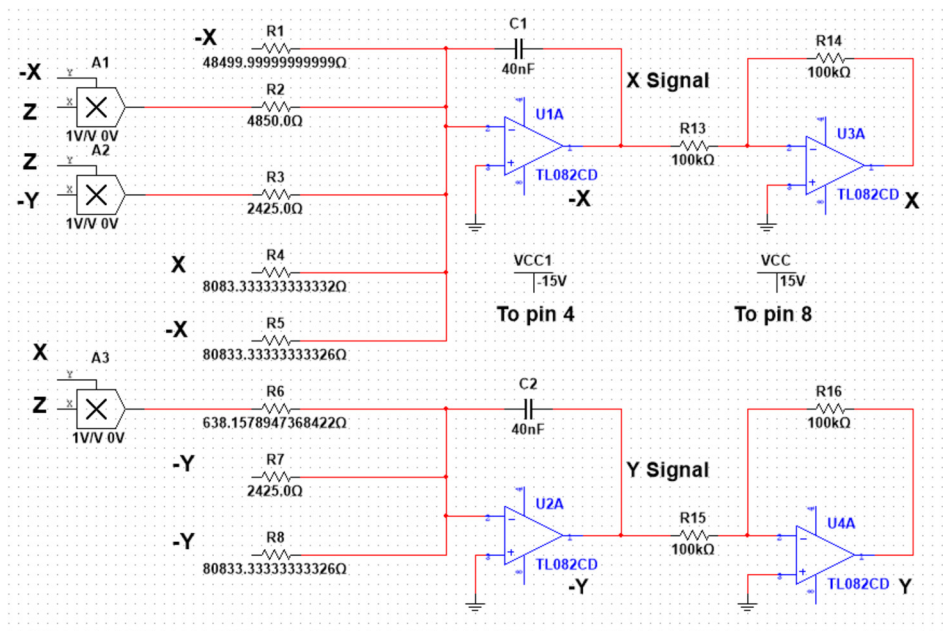


FIGURE 8.8 Electronic circuit of aggregated system (8.5).

8.4 Cryptography and security analysis

In this section, the chaotic data extracted from system (8.5) are used for the secure data protocols at fractional value 0.98 for voice and image data. The security protocols are carried out by using the conventional bitxor operation between the data extracted from the chaotic

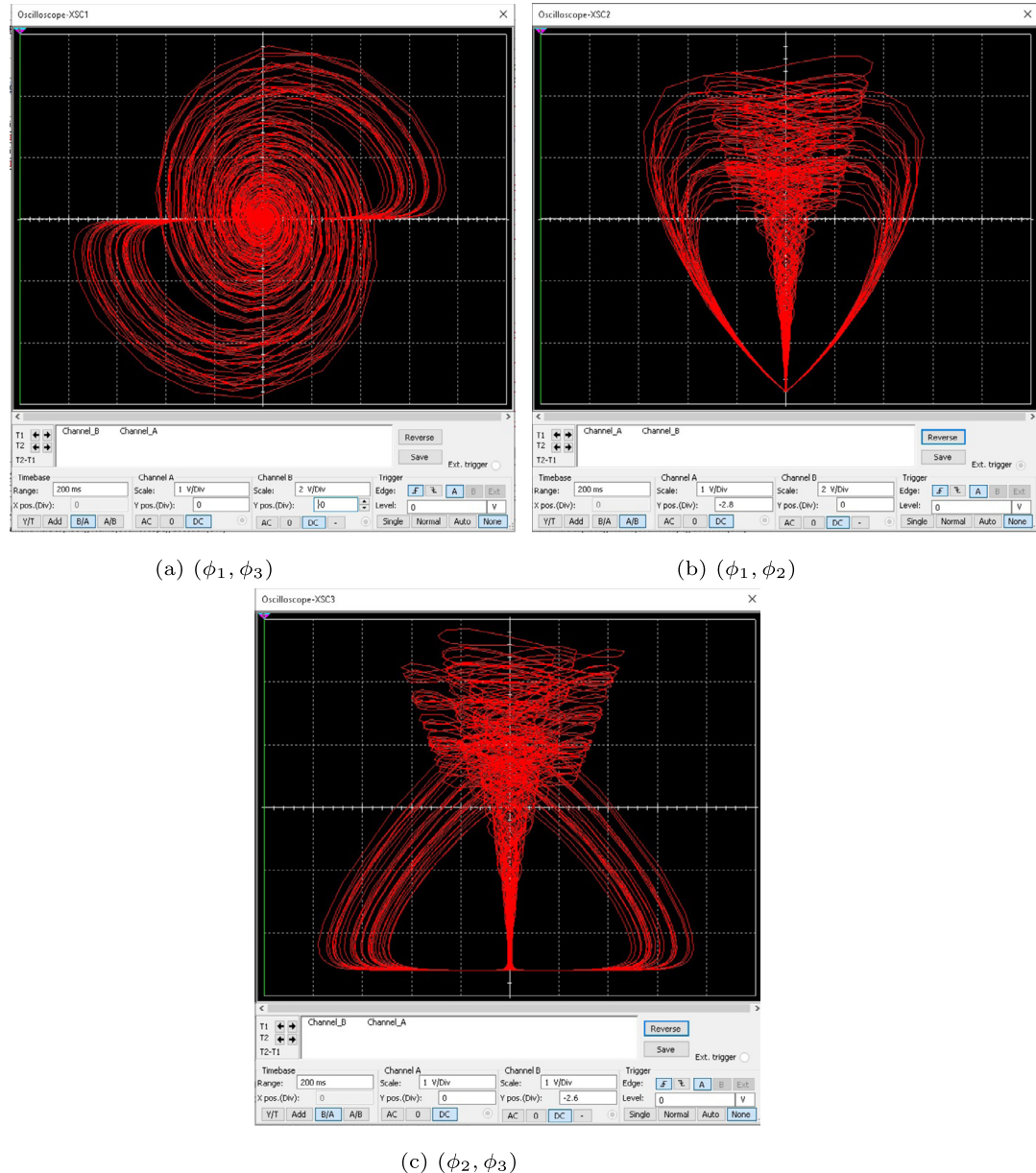


FIGURE 8.9 Oscilloscope results of system (8.5) at $\gamma = 0.98$.

TABLE 8.4 The P -values test result (NIST-800-22) of new aggregated system (8.5) at $\gamma = 0.98$.

Statistic test	<i>P</i> -Value			Result
	$\phi_1(\tau)$	$\phi_2(\tau)$	$\phi_3(\tau)$	
Frequency Monobit	0.782788	0.501665	0.619470	Eligible
Frequency Block	0.748832	0.277538	0.101152	Eligible
Runs	0.438904	0.737985	0.941962	Eligible
Longest Runs Ones 10000	0.092895	0.664352	0.433919	Eligible
Matrix Rank	0.233992	0.979288	0.429229	Eligible
Spectral	0.834115	0.669211	0.348125	Eligible
Nonoverlapping	0.827392	0.791559	0.021093	Eligible
Overlapping	0.408959	0.468407	0.858465	Eligible
Maurer's Universal Statistic	0.770565	0.034061	0.595002	Eligible
Complexity	0.493226	0.286453	0.681459	Eligible
Serial 1	0.190305	0.188522	0.697022	Eligible
Serial 2	0.180157	0.409663	0.351087	Eligible
Entropy	0.455580	0.403304	0.693955	Eligible
Cumulative Sums	0.544613	0.419801	0.658207	Eligible
Random Excursions at $x = -4$	0.125471	0.496103	0.898545	Eligible
Excursions Variant $x = -9$	0.266058	0.103780	0.366513	Eligible
Cumulative Sums	0.340590	0.745427	0.980004	Eligible
Lempelziv Compression	1	1	1	Eligible

system and the data of the file to be encrypted. We first endorse the fact that our chaotic system is remarkable in terms of randomness of data, for which we calculate the P-values by the standard NIST 800-22 protocol. The NIST 800-22 test carried out for our aggregated chaotic system is tabulated in Table 8.4, and all tests are in good agreement with standards of nonlinearity. After the successful random number testing, we proceed toward the encryption of voice data presented in Figs. 8.10 and 8.11. Figs. 8.10(a–c) represent the original, encrypted, and decrypted voice plots, and the encrypted data are full of fuzziness, which represents a good security tool. Figs. 8.11(a–c) are the spectrograms corresponding to the voice data represented in Figs. 8.10(a–c). The security is then applied to our image having R, G, and B data using bitxor generated between R, G, and B data along with our presented aggregated chaotic data as a key. Figs. 8.12(a–c) and 8.13(a–c) are image scrambling with original, encrypted, and decrypted figures for our selected images. The encryption portion for Figs. 8.12b and 8.13b is again a highly haphazard pixel, which shows that the data are perfectly hidden and secure. To examine the image encryption more in delineate manner, we plot histograms for our encrypted images shown in Figs. 8.14(a–c) and 8.15(a–c). The figure images in Figs. 8.13(b) and 8.13(c) are in absolute agreement for security applications, as in these figures the histogram data are distributed uniformly. The image and voice encryption are carried out in Python and are linked in as <https://doi.org/10.5281/zenodo.3693098> [36]. Lastly, we present the security application of our chaotic data to the text document in Pdf format. The day-to-day data file transfer in emails and other data transfer facilities can be made secure by using cryptography. Figs. 8.16(a–c) are the images of our encrypted Pdf text file with original, encrypted,

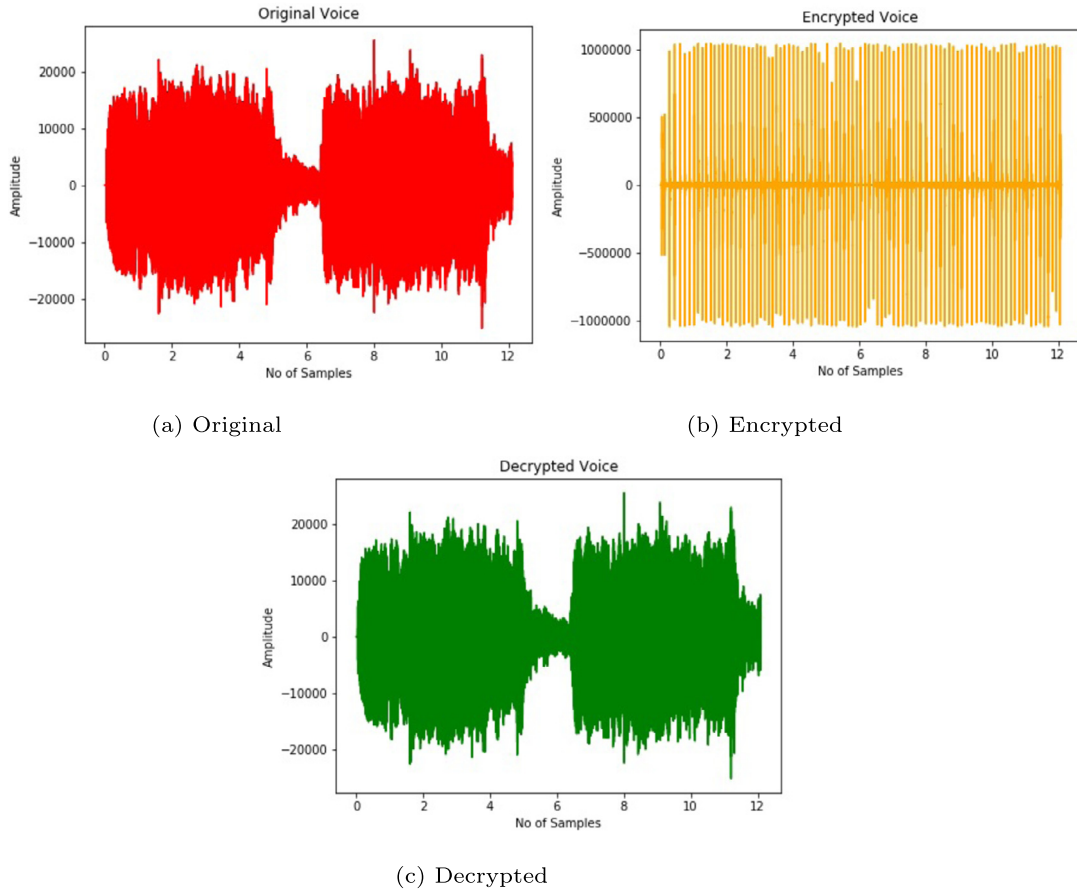


FIGURE 8.10 Original, encrypted, and decrypted voice signals.

and decrypted views. The encrypted view is successfully fused up with our system (8.5) for $\gamma = 0.98$, and only the key holder will be able to see the information.

NPCR and UACI

The number of pixels change rate (NPCR) and unified average changing intensity (UACI) are two important parameters in image cryptography for better standards of encryption. The calculation of these quantities is carried out by the formula

$$D(k, l) = \begin{cases} 0, & C(k, l) = C^*(k, l), \\ 1, & C(k, l) \neq C^*(k, l), \end{cases}$$

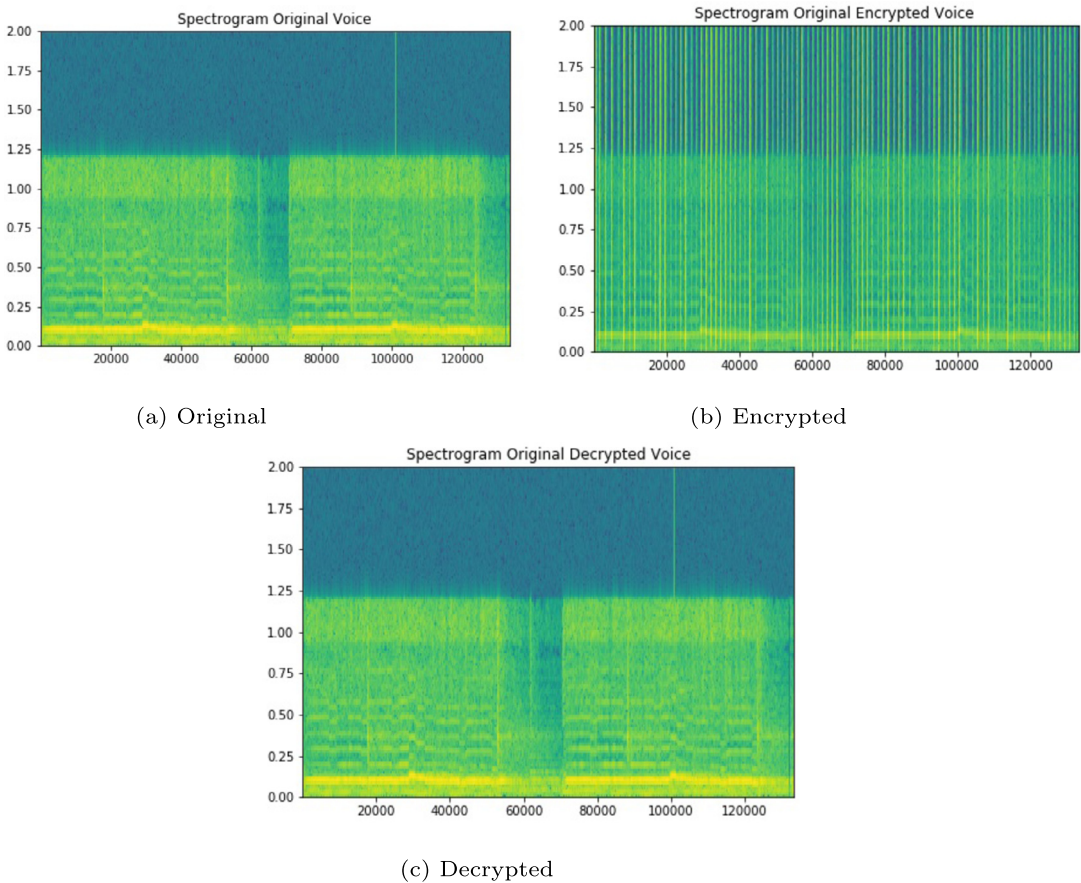


FIGURE 8.11 Spectrogram of original, encrypted, and decrypted voices.

$$NPCR = \sum_{k=1}^M \sum_{l=1}^N \left[\frac{D(k, l)}{MN} \right] \times 100\%,$$

where $C(k, l)$ and $C^*(k, l)$ characterize the pixel values for the original and encrypted images, respectively.

The unified average changing intensity (UACI) indicates the average value of the changed pixel and is defined as

$$UACI = \sum_{i=1}^M \sum_{j=1}^N \left[\frac{|C_1(i, j) - C_2(i, j)|}{255 \times M \times N} \right] \times \%.$$

For good encryption, NPCR value will be at least 99.6%, and UACI with more than 30%.

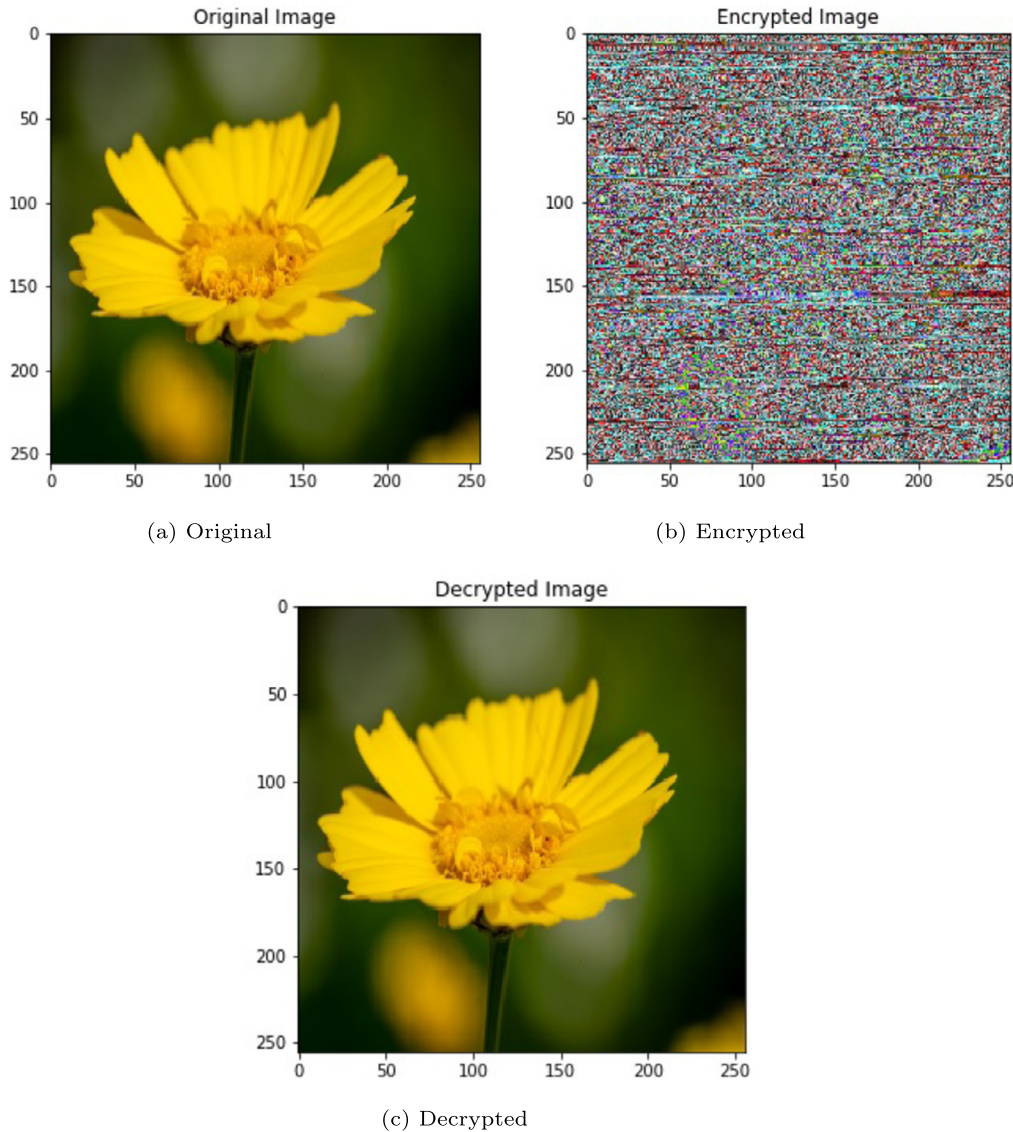


FIGURE 8.12 Original, encrypted, and decrypted flower images.

Correlation

The adjacent pixel relationship in an image is evaluated from the correlation analysis and is given by

$$\text{Correlation} = \sum_{j,k} \frac{(j - \eta_j)(k - \eta_k)p(j, k)}{\sigma_j \sigma_k}.$$

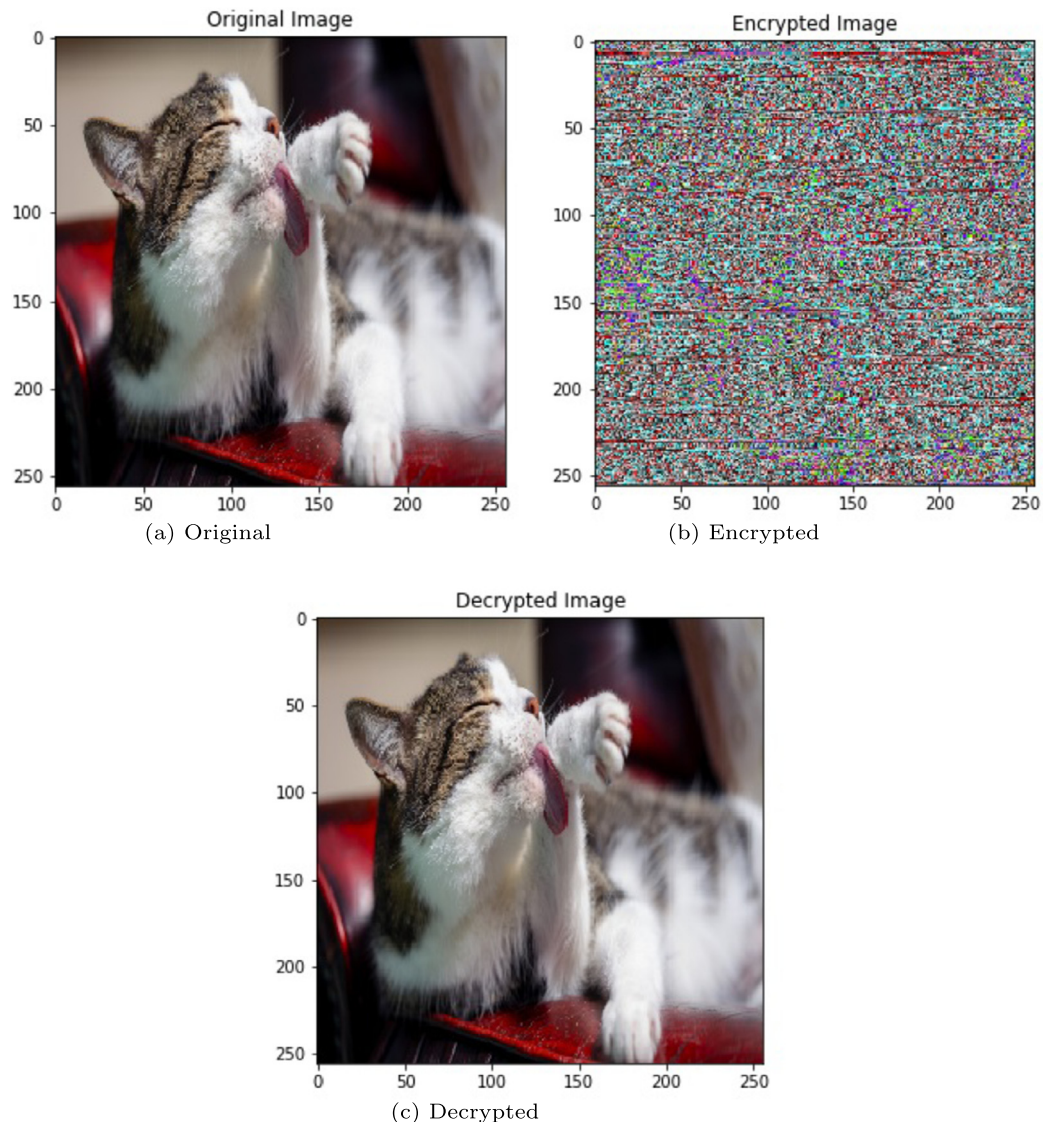


FIGURE 8.13 Original, encrypted, and decrypted cat images.

Mean square error (MSE)

The mean square error (MSE) is calculated to make sure that the original and decrypted images are in variations or not. The lesser the MSE between two images, the better the decryption; it is defined as

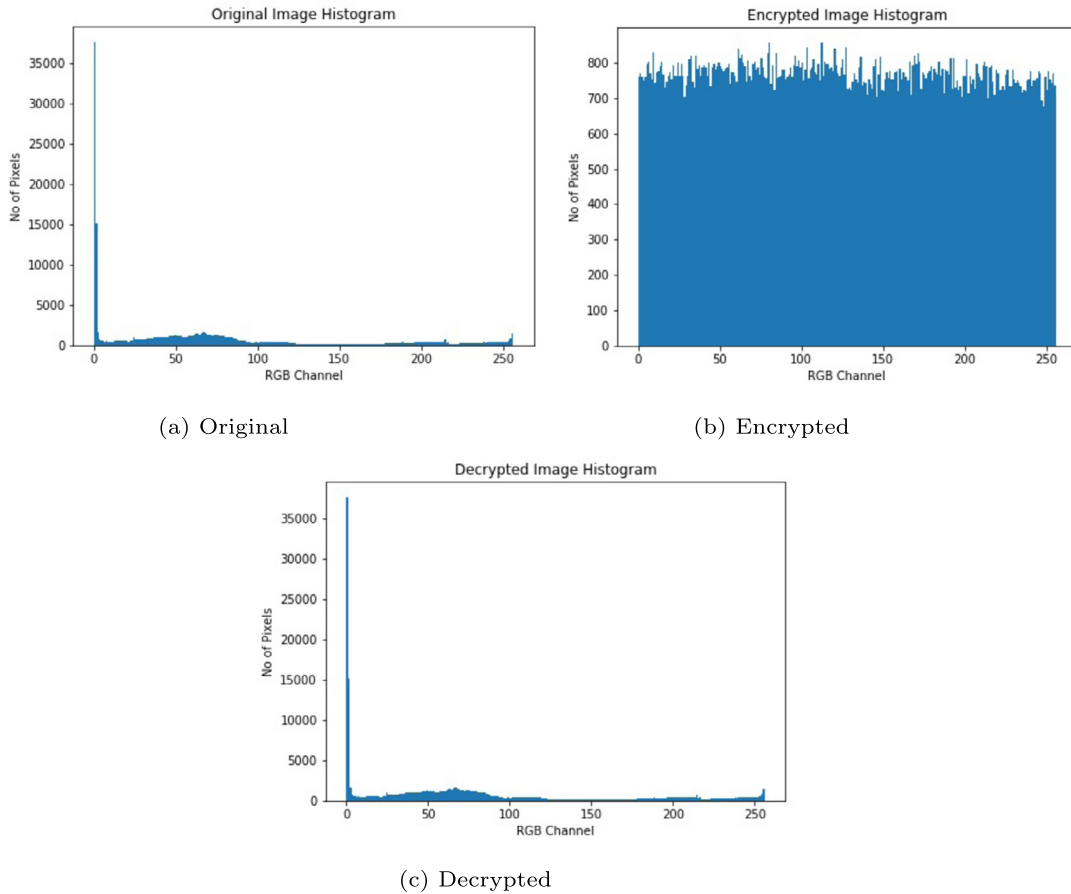


FIGURE 8.14 Original, encrypted, and decrypted histograms of flower images.

$$MSE(q_1, q_2) = \frac{1}{MN} \sum_{i=0}^{M-1} \sum_{j=0}^{N-1} (q_1(i, j) - q_2(i, j))^2,$$

where $q_1(i, j)$ and $q_2(i, j)$ indicate the original and decrypted images, respectively.

Peak signal-to-noise ratio (PSNR)

The inverse of the root mean square error (MSE) is the peak signal-to-noise ratio (PSNR)

$$PSNR = 10 \log_{10} \frac{(2^n - 1)^2}{MSE}.$$

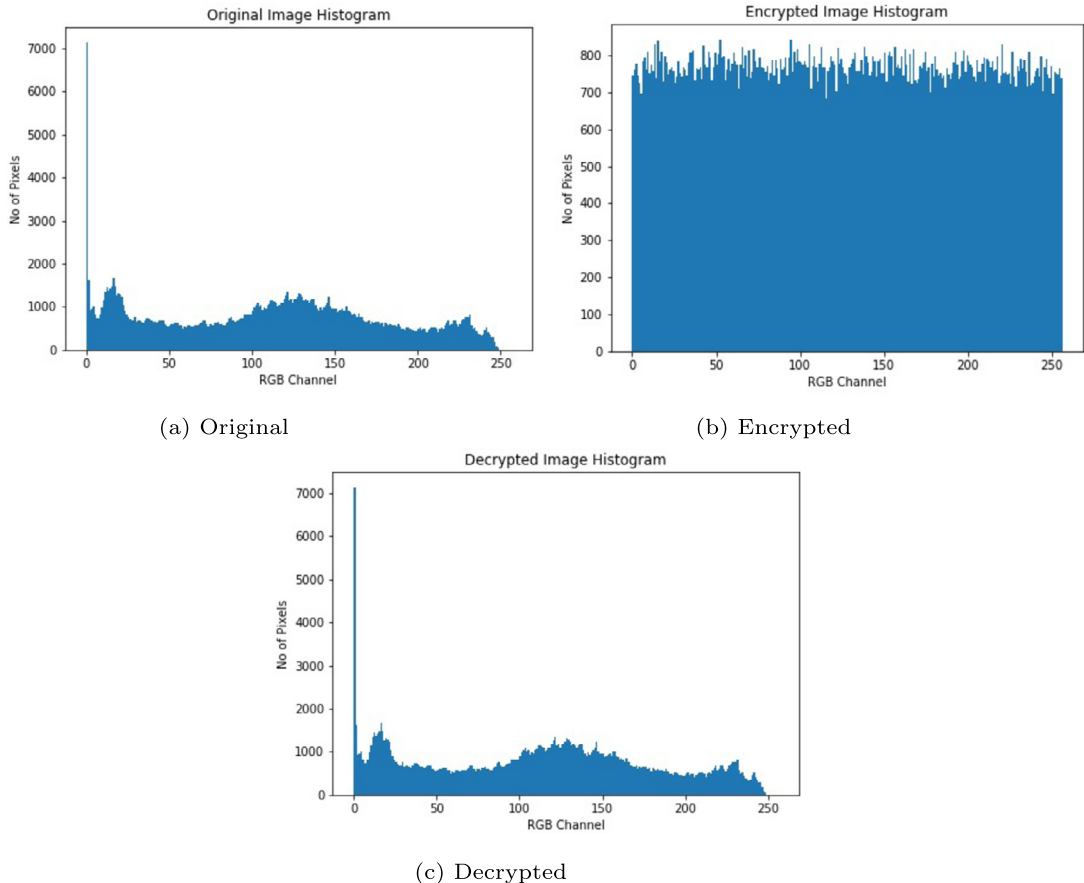


FIGURE 8.15 Original, encrypted, and decrypted histograms of cat images.

The better the PSNR, the better the encryption. The noise quality of the image is high when calculating PSNR.

Entropy

The disorder in a system is known as the entropy, which gives the level of arbitrariness and randomness in the system. In an image, we apply this on pixels of selected data by using the formula

$$H(s) = - \sum_{j=0}^{2^N-1} p(s_j) \log \left(\frac{1}{p(s_j)} \right),$$

where N is the number of bits, and p is the probability of image pixels. Analysis of the results for images is tabulated in Tables 8.5 and 8.6 for (NPCR, UACI, correlation analysis,

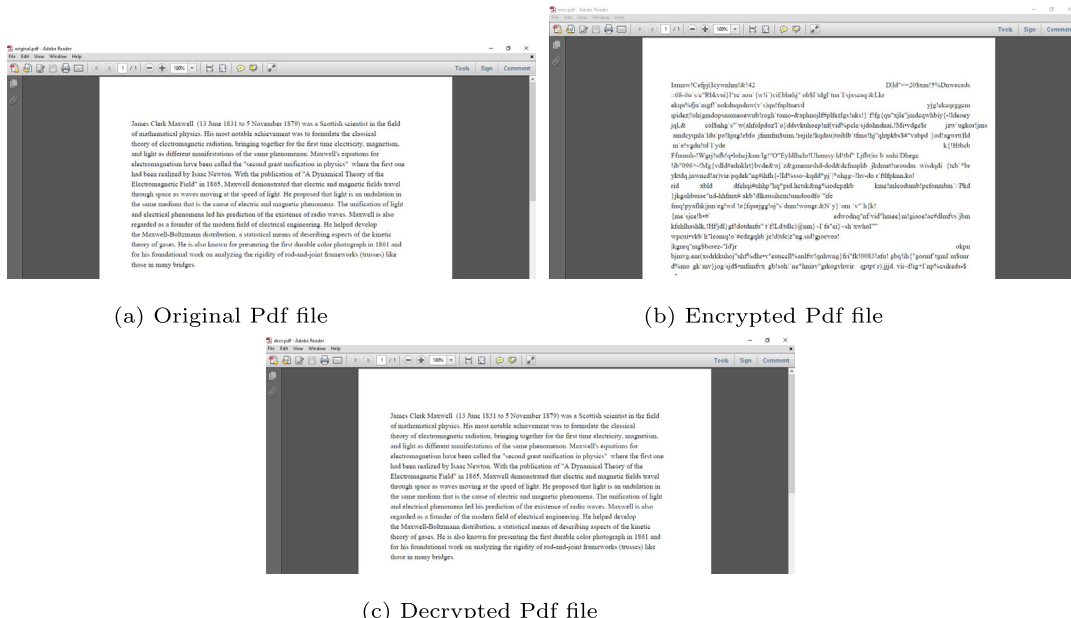


FIGURE 8.16 Original, encrypted, and decrypted Pdf files.

TABLE 8.5 Results of PSNR, MSE NPCR, UAIC, and correlation.

Image	Dimension	MSE	PSNR	NPCR (%)	UAIC (%)	Correlation	
						Original image	Encrypted image
Flower	256×256	0.00001	27.98051	99.41355	34.87079	0.98915	0.33668
Cat	256×256	0.00001	27.93915	99.57224	29.53447	0.96605	0.27608

PSNR, MSE) and entropy, respectively. The two unit (256×256) images (flower and cat) were processed through these tests and passed successfully. The NPCR and UAIC are in good agreement for both images, and the correlation analysis results show us that the original flower and cat data pixels are highly correlated with each other, whereas the encrypted correlation is collapsed to a very low number. The root mean square of original and decrypted images is 0.00001, showing us that the scrambled image is returned successfully as the original one without any data loss. The PSNR result is very high, representing the fact that the original and encrypted images have a huge amount of noise between their pixels. We then calculate the entropy of our cryptographic images at the scale R, G, and B for both images, which is tabulated in Table 8.6. From this result we can see that the pixels of original and encrypted images have good amount variation, showing us that the data are strongly encrypted. We also present the entropy of encrypted and original images using a color map, which is again in good agreement in terms of security.

TABLE 8.6 Results of Entropy.

Image	Entropy		Entropy Image	
	Original	Encrypted	Original	Encrypted
Flower	R	7.517365306220164	7.863384388116977	
	G	7.455778617716194	7.8402560696143775	
	B	3.7000180119074715	7.760090794877891	
Cat	R	7.834291850837606	7.94272951577872	
	G	7.761028648575783	7.9400110988243995	
	B	7.806731097234409	7.78077439475547	

8.5 Conclusion

In this chapter, we present the accretion of two chaotic systems with fractional derivative technique for complex systems sensitive to initial conditions. The dynamical parameters of our system are studied extensively with phase portraits, eigenvalues, Lyapunov exponents, and Poincaré maps. The system is established for perceptible application for generating the same random chaotic signals through electronic components as depicted from numerical solution of our accrue equation. The randomness through fractional order is well used in doing cryptography for scrambling voice, image, and Pdf file. The future possibilities of the work are as follows.

- The new accrue system has different stability points from the previous unmerged systems.
- Complex chaotic data are generated with the addition of γ , with dissimilar Kaplan–Yorke dimensions of different order.
- Electronic realization is in good agreement depicting the great resemblance in numerical solution and circuit signals.
- Cryptography of image, voice, and Pdf text file is done to ensure the security application to this new developed system. Other files such as Pdf image file and Docx file can also be encrypted.
- Tests for standard security protocols are taken into account for image quality of encryption.

References

- [1] H. Weidenmüller, G. Mitchell, Random matrices and chaos in nuclear physics: nuclear structure, *Reviews of Modern Physics* 81 (2) (2009) 539.
- [2] C.W. Horton, L.E. Reichl, *Statistical Physics and Chaos in Fusion Plasmas*, 1984.
- [3] Y. Cho, T. Umeda, Chaos in laser oscillations with delayed feedback: numerical analysis and observation using semiconductor lasers, in: *International Quantum Electronics Conference*, Optical Society of America, 1984, p. WEE2.
- [4] M. Kyriazis, Applications of chaos theory to the molecular biology of aging, *Experimental Gerontology* 26 (6) (1991) 569–572.
- [5] D.S. Coffey, Self-organization, complexity and chaos: the new biology for medicine, *Nature Medicine* 4 (8) (1998) 882–885.

- [6] R.M. May, Chaos and the dynamics of biological populations, Nuclear Physics. B, Proceedings Supplement 2 (1987) 225–245.
- [7] D. Guegan, Chaos in economics and finance, Annual Reviews in Control 33 (1) (2009) 89–93.
- [8] B. LeBaron, Chaos and nonlinear forecastability in economics and finance, Philosophical Transactions of the Royal Society of London. Series A: Physical and Engineering Sciences 348 (1688) (1994) 397–404.
- [9] C. Bai, H.-P. Ren, M.S. Baptista, C. Grebogi, Digital underwater communication with chaos, Communications in Nonlinear Science and Numerical Simulation 73 (2019) 14–24.
- [10] G.D. Vanwiggeren, R. Roy, Communication with chaotic lasers, Science 279 (5354) (1998) 1198–1200.
- [11] N. Khodor, J.-P. Cances, V. Meghdadi, R. Quéré, Performances of chaos coded modulation schemes based on high dimensional LDPC mod-map mapping with belief propagation decoding, in: 2010 7th International Symposium on Communication Systems, Networks & Digital Signal Processing (CSNDSP 2010), IEEE, 2010, pp. 217–222.
- [12] J. Yu, Y.-D. Yao, Detection performance of chaotic spreading LPI waveforms, IEEE Transactions on Wireless Communications 4 (2) (2005) 390–396.
- [13] E. Rosa Jr, S. Hayes, C. Grebogi, Noise filtering in communication with chaos, Physical Review Letters 78 (7) (1997) 1247.
- [14] A. Bobtsov, A. Pyrkin, N. Nikolaev, O. Slita, Stabilization of a chaotic Van der Pole system, IFAC Proceedings Volumes 41 (2) (2008) 15143–15147.
- [15] Z.-M. Ge, C.-Y. Ou, Chaos in a fractional order modified Duffing system, Chaos, Solitons and Fractals 34 (2) (2007) 262–291.
- [16] Y. Yu, H.-X. Li, S. Wang, J. Yu, Dynamic analysis of a fractional-order Lorenz chaotic system, Chaos, Solitons and Fractals 42 (2) (2009) 1181–1189.
- [17] L.O. Chua, M. Itoh, L. Kocarev, K. Eckert, Chaos synchronization in Chua's circuit, Journal of Circuits, Systems, and Computers 3 (01) (1993) 93–108.
- [18] L.-J. Sheu, H.-K. Chen, J.-H. Chen, L.-M. Tam, W.-C. Chen, K.-T. Lin, Y. Kang, Chaos in the Newton–Leipnik system with fractional order, Chaos, Solitons and Fractals 36 (1) (2008) 98–103.
- [19] V. Sundarapandian, S. Sivaperumal, Anti-synchronization of the hyperchaotic Lorenz systems by sliding mode control, International Journal on Computer Science and Engineering 3 (6) (2011) 2450–2457.
- [20] S. Vaidyanathan, S. Sampath, Hybrid synchronization of hyperchaotic Chen systems via sliding mode control, in: International Conference on Computer Science and Information Technology, Springer, 2012, pp. 257–266.
- [21] M.M. Al-Sawalha, M.S.M. Noorani, Application of the differential transformation method for the solution of the hyperchaotic Rössler system, Communications in Nonlinear Science and Numerical Simulation 14 (4) (2009) 1509–1514.
- [22] I. Podlubny, Fractional Differential Equations: an Introduction to Fractional Derivatives, Fractional Differential Equations, to Methods of Their Solution and Some of Their Applications, Elsevier, 1998.
- [23] K.B. Oldham, J. Spanier, The Fractional Calculus, Mathematics in Science and Engineering, vol. 111, 1974.
- [24] M. Du, Z. Wang, H. Hu, Measuring memory with the order of fractional derivative, Scientific Reports 3 (1) (2013) 1–3.
- [25] V.E. Tarasov, V.V. Tarasova, Long and short memory in economics: fractional-order difference and differentiation, arXiv preprint, arXiv:1612.07903.
- [26] Y. Ding, Z. Wang, H. Ye, Optimal control of a fractional-order HIV-immune system with memory, IEEE Transactions on Control Systems Technology 20 (3) (2011) 763–769.
- [27] C.A. Monje, B.M. Vinagre, V. Feliu, Y. Chen, Tuning and auto-tuning of fractional order controllers for industry applications, Control Engineering Practice 16 (7) (2008) 798–812.
- [28] R. Meng, D. Yin, C.S. Drapaca, Variable-order fractional description of compression deformation of amorphous glassy polymers, Computational Mechanics 64 (1) (2019) 163–171.
- [29] R.L. Magin, C. Ingo, L. Colon-Perez, W. Triplett, T.H. Mareci, Characterization of anomalous diffusion in porous biological tissues using fractional order derivatives and entropy, Microporous and Mesoporous Materials 178 (2013) 39–43.
- [30] D. Cowan, G. Cooper, Separation filtering using fractional order derivatives, Exploration Geophysics 36 (4) (2005) 393–396.
- [31] N.A. Khan, T. Hameed, M.A. Qureshi, S. Akbar, A.K. Alzahrani, Emulate the chaotic flows of fractional jerk system to scramble the sound and image memo with circuit execution, Physica Scripta 95 (6) (2020) 065217.

- [32] N.A. Khan, M.A. Qureshi, T. Hameed, S. Akbar, S. Ullah, Behavioral effects of a four-wing attractor with circuit realization: a cryptographic perspective on immersion, *Communications in Theoretical Physics* 72 (12) (2020) 125004.
- [33] A. Sambas, S. Vaidyanathan, M. Mamat, M. Sanjaya, S. Yuningsih, K. Zakaria, Analysis, control and circuit design of a novel chaotic system with line equilibrium, *Journal of Physics. Conference Series* 1090 (2018) 012010.
- [34] H.-K. Chen, C.-I. Lee, Anti-control of chaos in rigid body motion, *Chaos, Solitons and Fractals* 21 (4) (2004) 957–965.
- [35] A. Wolf, J.B. Swift, H.L. Swinney, J.A. Vastano, Determining Lyapunov exponents from a time series, *Physica D: Nonlinear Phenomena* 16 (3) (1985) 285–317.
- [36] M.A. Qureshi, Encryption-Python-codes: release of voice and image encryption in Python, Zenodo, <https://doi.org/10.5281/zenodo.3693098>.